Development and Laboratory Testing of a CubeSat-Compatible Staged Ionic-Liquid Electrospray Propulsion System

Development and Laboratory Testing of a CubeSat-Compatible Staged Ionic-Liquid Electrospray Propulsion System

Gustav M. Pettersson*, Oliver Jia-Richards†, and Paulo C. Lozano‡
Massachusetts Institute of Technology, Cambridge, MA 02139, USA

Advances in propulsion systems are key to enabling independent deep-space CubeSat missions. Currently available electric propulsion technologies require relatively high power and thereby heavy power generation systems, severely limiting their utility for missions going away from the Sun. The ionic-liquid electrospray is known to have high power efficiency but a relatively short lifetime in its present state, limiting the total impulse available in such systems. This lifetime limit can be overcome by using several stages of thrusters, which are used in sequence to multiply the total system lifetime. In this paper, we present the design details and laboratory testing results for a staging system that is compatible with the CubeSat standard. This system will later be demonstrated in space on the STEP-1 satellite, which could enable an exciting new era of accessible CubeSat exploration around the solar system.

Nomenclature

c	=	Effective exhaust velocity of propulsion system, m/s
d	=	Hold-down wire diameter, m
E	=	Elastic (Young's) modulus, Pa
k	=	Stiffness (spring constant), N/m
L	=	Hold-down wire length, m
m_0	=	Spacecraft initial wet mass, kg
m_{dry}	=	Propulsion system dry mass, kg
m_{pay}	=	Spacecraft payload mass, kg
$\mathbb{P}$	=	Electrical power of propulsion system, W
α	=	Specific power of electricity generation, W/kg
Δv	=	Velocity increment from propulsion, m/s

I. Introduction

CubeSats have matured into roles beyond their initial educational and technology demonstration purposes. By their quick turnaround and low cost, they have enabled new science mission profiles and commercial satellite operations. In recognition of this, a report on achieving science with CubeSats was commissioned and aimed at identifying key technology gaps for CubeSats [1]. This report concluded that propulsion was one of the highest priority areas of development. There is a strong push to develop a variety of different electric propulsion technologies for the CubeSat form factor such as ionic-liquid electrospray thrusters [2, 3], field-emission electric propulsion (FEEP) [4], and radio-frequency (RF) ion thrusters [5]. These different propulsion technologies could offer large Δv capabilities (over 1 km/s) for CubeSats, and in some cases have already been demonstrated in low-Earth orbit [6]. However, several technology hurdles need to be addressed before these propulsion systems are applied to deep-space missions. The viability of deep-space CubeSats was demonstrated with the *MarCO* mission to Mars [7] and several new CubeSat missions are now slated for launch outside Earth orbit [8]. However, the low power efficiency of many electric propulsion technologies at the CubeSat scale severely limits the potential payload for missions that travel away from the Sun. This low power efficiency is typically due to power requirements outside of the power used to accelerate ions. Some examples include heating of the propellant, ionisation of the propellant, and neutralisation of the emitted ion beam with an external neutraliser.

*PhD Candidate, Department of Aeronautics and Astronautics.
†Doctoral Candidate, Department of Aeronautics and Astronautics.
‡Professor, Department of Aeronautics and Astronautics.

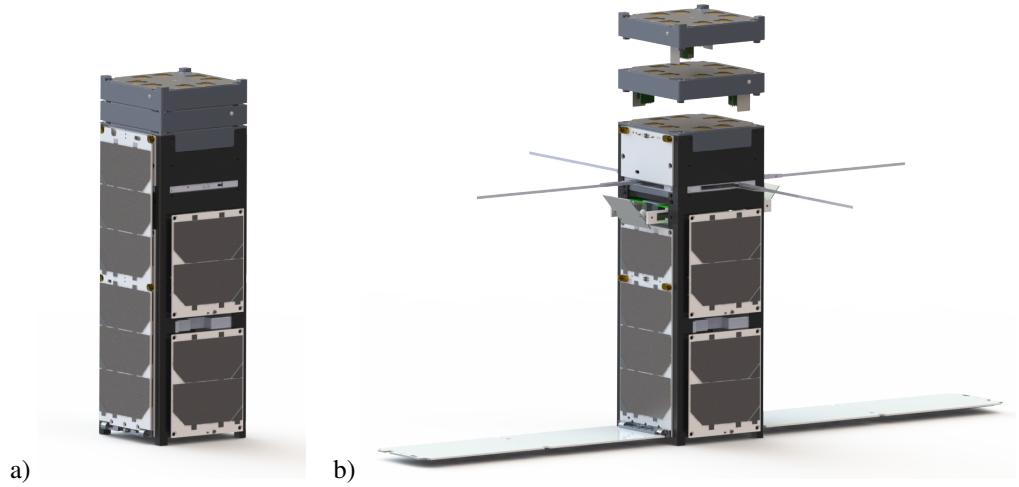

Fig. 1 The STEP-1 CubeSat computer model. a) Stowed for launch. b) Fully deployed.

Ionic-liquid electrospray thrusters hold many advantages that could provide a potential solution to the problem of low power efficiency for CubeSat-compatible electric propulsion. Ionic liquids are room-temperature molten salts and are effectively "pre-ionised", eliminating the energy expenditure for propellant heating and ionisation. In addition, the ability to fire ionic-liquid electrospray thrusters in a bipolar configuration from a single propellant supply eliminates the need for an external neutraliser; the positive and negative emitted thruster currents combine to preserve spacecraft neutrality or desired charge [9]. These advantages allow the demonstrated power efficiency of ionic-liquid electrospray thrusters to reach 65% [3] and could enable deep-space exploration with CubeSats. However, the lifetime of the current generation of electrospray thrusters is insufficient to enable deep-space missions. While lifetime limiting mechanisms and mitigation for electrosprays are actively studied and expected to bring lifetime improvements in the future [10], considering alternative methods for improving the overall lifetime of the propulsion system can bring the viability of deep-space CubeSats sooner.

Staging of ionic-liquid electrospray thrusters, analogous to launch vehicle staging, has been proposed as a potential solution to the lifetime limitations [11]. A stage-based system would leverage the low mass and volume of ionic-liquid electrospray thrusters to bypass the lifetime limitations of an individual thruster, and increase the overall lifetime of the propulsion system. As the thrusters on each stage reach their lifetime limits, the stage is ejected from the spacecraft in order to expose a new stage and continue the mission. Stage-based systems of ionic-liquid electrospray thrusters have been studied for missions to the Moon [11] or near-Earth asteroids [12]. A theoretical framework for analysing stage-based systems has also been developed to study their application to a wider range of missions [13].

Here, we present ongoing work on the Staged Electrospray Pathfinder 1 (STEP-1) project which aims to develop practical and scalable hardware for a staged-based system with a low-Earth orbit (LEO) technology demonstration. A laboratory demonstration of prototype hardware has previously been conducted [14], but it is critical that this technology can be implemented in a flight-compatible manner for the CubeSat form factor. With STEP-1 we will also perform testing and characterisation of ionic-liquid electrosprays on-orbit to further their maturity. Our goal is to effectively and quickly provide the building blocks for future deep-space missions, but STEP-1 itself is not designed to maximise Δv. STEP-1 was recently selected for launch through NASA's CubeSat Launch Initiative program.

II. STEP-1 Mission and Design

The STEP-1 mission's purpose is to develop and mature a staging system suitable for high Δv deep-space CubeSat missions. A 3U ($10 \times 10 \times 34\,\mathrm{cm}^3$) CubeSat deployed to LEO was selected to keep cost and development time low, while allowing sufficient payload volume and power for a substantial propulsion unit. The bus is shown in Fig. 1 and consists of 1.5U commercial off-the-shelf subsystems, a 1U propulsion payload, and a 0.3U camera payload. A semi-custom structure and solar panels were designed to accommodate the payloads. The camera payload extends two mirrors from the bus to provide a clear view of the propulsion payload and will record the staging events on orbit to determine separation success and dynamics.

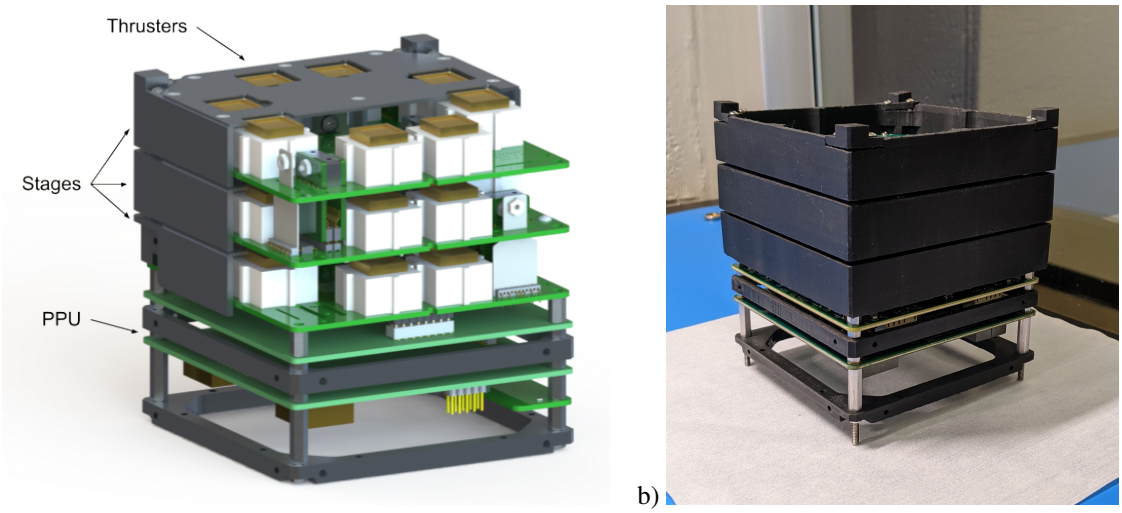

Fig. 2 The STEP-1 propulsion system. a) Cutaway computer rendering. b) Assembled prototype.

The STEP-1 propulsion unit is designed to leverage the strengths of the CubeSat platform, namely high standardisation and flexibility, with low cost, mass, and volume. To achieve this, a three-stage propulsion module was selected where the middle stage may be replicated any number of times and all elements of the staging are modular and scalable. The staging system is electrically "invisible" to the thrusters and power processing unit (PPU), which decouples the further development of these technologies from each other. The stages on STEP-1 include eight thrusters each and are based on previously published designs for single-stage flight projects [15, 16] and a flight-heritage PPU is used.

III. STEP-1 Staging System Design

The STEP-1 staging system design is driven to occupy the smallest feasible surface area on each stage while minimising the volume and mass penalty introduced with each extra stage as compared to a larger single-stage. Shown in Fig. 2, the three stages are spaced by 20 mm and include the PPU in a 1U ($10 \times 10 \times 11$ cm^3) volume. The staging system controller is mounted inside the standard satellite bus subsystem stack. The stages are mated and aligned by conical surfaces in each corner of the structural walls which also house separation springs. Four stainless steel hold-down wires connect the stages and are dimensioned to transfer the structural launch loads through the payload to the bus. Signals are routed within the stack through a compliant interstage connector and interruptor system in the corner of each board. The routing system is designed to avoid electrical addressing to the stages by passively and mechanically connecting thruster power and control signals to the uppermost stage only. Staging is performed by fusing the hold-down wires and the physical separation of the stages actuate the routing system to connect the next stage. Fig. 3 shows a diagram of the staging and routing process. The STEP-1 design provides eight high-voltage thruster connections, requires less than 20 cm^2 area and 150 g penalty mass per stage, and can be scaled to larger future systems with small penalty increases.

The hold-down and release mechanism concept selection was previously studied [17] and demonstrated in a vacuum environment [14]. A simplified miniature fuse wire release mechanism [18] was selected because of its compactness and high load carrying capacity, while avoiding potentially hazardous technologies such as pyrotechnics. The stainless steel (type 304) fuse wires are actuated by supplying current from a supercapacitor, rapidly heating them to separate the stages. The second generation of this concept was developed in STEP-1 to conform with the CubeSat standard and further optimise the design. The first generation design [17] nested the fuse wire and separation springs inside a ceramic standoff in each corner of the stages. Since this limited the load-carrying capacity of the stages and required relatively large board spacing the fuse wire was moved to an adjacent wire block on the circuit board and the ceramic interface was replaced with conical mating features directly integrated into the metallic structure of the stage, shown in Fig. 4a. The wire blocks were subsequently moved from the corners to the middle of the stages to relax separation timing requirements; allowing a simplified control strategy. The hold-down wire diameter was selected by performing finite element analysis on the staging system with a worst-case loading, see Section V.A. It is desirable to limit the heating of the hold-down wire to a specific short segment to control the severance location and reduce the power required. In [18] this was performed by selectively thinning the wire to concentrate heating. We perform the same function by adding a

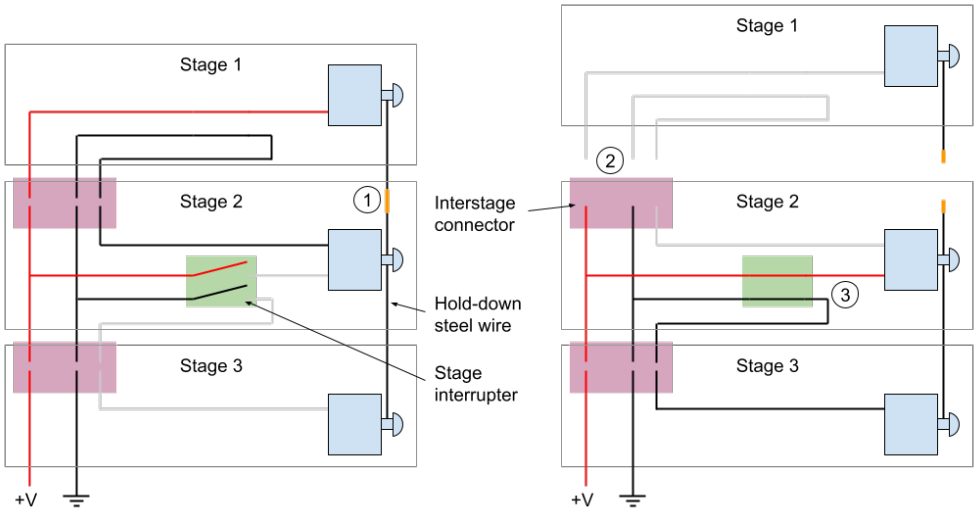

Fig. 3 Simplified diagram of the staging process. First, the hold-down wire is severed and the upper stage starts to separate. Second, after approximately 1 mm movement the interstage disconnects. Third, after approximately 3 mm movement the lower stage interrupter connects and the system is ready to operate again. The middle stage may be repeated any number of times or omitted to tailor the system for a specific mission.

thin tube of stainless steel as a sleeve to the wire which reduces the resistance and increases the thermal mass of the sleeved segment. The sleeve is crimped to the wire and subsequently wrapped with a polytetrafluoroethylene (PTFE) heat shrink tube to insulate the wire, shown in Fig. 4b. The separation springs were selected to guarantee a separation speed of less than 1 m/s and to be the last points of contact between the stages.

The stage interconnect system uses 20 spring-loaded pogo-pins and conical targets to provide a compliant and resilient connection, shown in Fig. 4c. The pogo-pins allow relative vertical motion up to 1.4 mm to ensure reliable electrical connections throughout the staging process. Using standard board-to-board pins and sockets was also studied for the interconnection. While the density and customisable height offered by pins and sockets are desirable, the static friction would require strong separation springs to overcome and lead to excessive separation speed. The pogo-pin connectors are mounted on daughterboards extending down from each stage which are adjusted in length to accommodate any stage spacing. Two rows of small 1.27 mm pitch connectors were chosen for the interconnect to preserve space and the connector pins adjacent to each high-voltage signal are depopulated to give sufficient isolation. The stage interrupter is a similar pogo-pin connector which is held open by a thin isolation sheet mounted to the structure of the stage above. The sheet is pulled out by the motion of the upper stage which connects the high-voltage thruster connections and produces a signal to reset the staging system and enable the telemetry circuits on the newly exposed stage. Through this interrupter and routing strategy the lower stages are physically inhibited from firing prematurely, and any number of stages can be added without any modifications. This choice of staging management ensures the staging technology developed here is flexible, modular, and scalable, properties highly desirable for CubeSat applications, at the expense of some complexity to the interstage connection. The isolation sheet is 0.5 mm thick and the desired material characteristics are high dielectric breakdown strength, low friction, and toughness. Initially, PTFE was selected because of its ductility and low friction, however, long-term testing showed signs of material creep which formed indentations under the force of the pins. The interrupter was changed to polyetheretherketone (PEEK) which passed creep testing and has similar dielectric strength.

IV. Methods

A. Structural finite element analysis

Finite element analysis (FEA) was performed in *SolidWorks 2019* on the payload structure. The model complexity was reduced by replacing all components on the circuit boards with a distributed mass load and filling all small holes. The interstage connectors and hold-down wires were simulated using spring elements preloaded to produce the correct

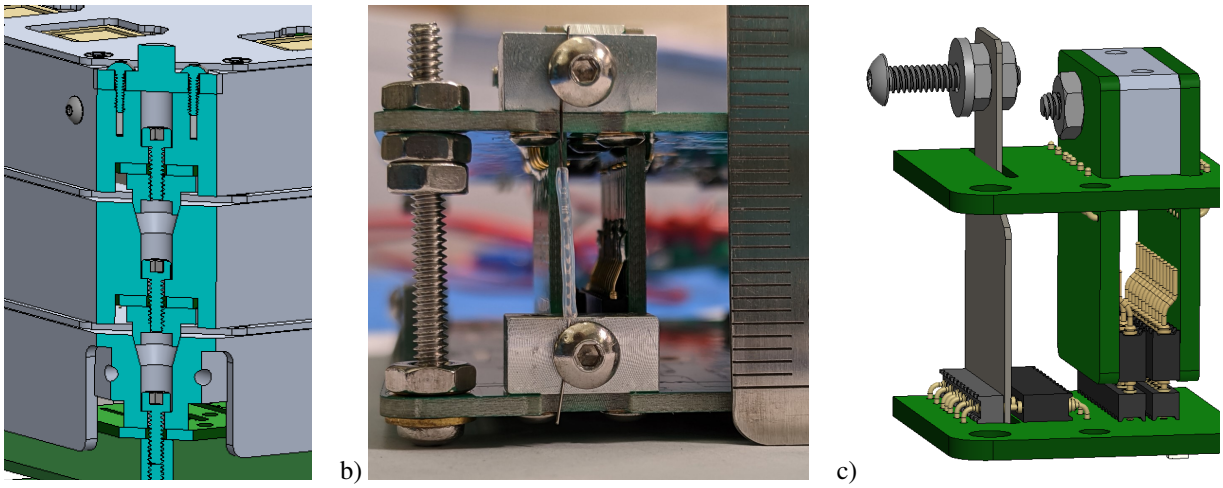

Fig. 4 Hold-down and release mechanism details. a) Cutaway view of the conical mating surfaces between stages; the voids house the separation springs (not shown). b) Hold-down wire after fusing with stainless steel and PTFE sleeves to control location. c) View of the interstage connectors and interrupter.

tension. Within each stage all components were fused into a single mesh. The interfaces between stages were simulated using a non-linear no-penetration boundary condition applied to the conical mating features. Mesh element sizes were 5 mm to 25 mm within the stages and approximately 2 mm at the mating interfaces.

The staging wire stiffness was calculated as:

$$k = \frac{\pi}{4}\frac{Ed^2}{L} \tag{1}$$

and the tension was confirmed by simulating the system without any external loads. The design load case was a distributed load of 320 N spread across the $+Y$ faces of the second and third stages with the first stage mounting holes fixed. This was selected to correspond to the worst-case scenario of a 4 kg CubeSat accelerated at 80 $\mathrm{m/s^2}$ being fully supported by the upper stages. The resulting force in each wire and the maximum deflection of the top stage were recorded. The wire diameter and tension were varied until a factor of safety of two and a deflection of less than 0.5 mm were attained.

B. Staging separation demonstration

An integrated two-stage prototype including a payload structure and staging HDRM representative for flight was assembled and demonstrated vertically. In this prototype, the hold-down wire tension was set by hand which is expected to impact the fuse timing. The fuse power was supplied by a benchtop power supply set to 3.5 V and the control electronics were supplied by a separate 5 V power supply. The fuse current and supply voltage were measured on the lower stage and video was recorded. The video camera was placed approximately 2 m away from the system to minimise perspective effects and an exposure time of 1 ms and a frame-rate of 120 Hz were used. The system was activated by manually connecting the fuse control signals and a light-emitting diode (LED) was connected to the activation signal to synchronise the data. The staging video was post-processed in *MATLAB* where the positions of the top corners of the stage were recorded for each frame. The pixel scale was calibrated using known dimensions of the staging system. The centre-of-mass distance travelled was taken as the average of the corner positions and the tilt angle was derived from their difference. The separation speed was determined by an energy balance and the resulting speed and tip-off rates were scaled to a stage mass of 200 g which is representative for flight.

C. Performance scaling

System-level propulsion performance was calculated for a future 6U CubeSat using a STEP-1-derived staged electrospray propulsion unit and several commercial state-of-the-art systems. The data is presented as available payload

mass for a desired mission Δv, given by:

$$m_{\text{pay}} = m_0 \exp\left(-\frac{\Delta v}{c}\right) - m_{\text{dry}} - \alpha^{-1}\mathbb{P} \tag{2}$$

with $m_0 = 12\,\text{kg}$. Comparisons were performed assuming $\alpha = 100\,\text{W/kg}$ at Earth, and with $\alpha = 16\,\text{W/kg}$ scaled to represent operation in the asteroid belt at 2.5 AU. Four commercial state-of-the-art systems were used for reference, with specification given in Table 1. Two performance outcomes for the electrospray were included, shown in Table 2, which correspond to the immediate target and near-future performance goals. A 64-thruster configuration with a base mass of 250 g for the power and control electronics and a stage mass penalty doubled from the STEP-1 results, 300 g, was assumed.

Table 1 Performance parameters for state-of-the-art comparison.

System	Thrust	Specific impulse	Power	Total impulse	Wet mass	Source
Iodine RF	1.1 mN	2150 s	75 W	31.6 kN s	2.78 kg	[19]
Indium FEEP	0.7 mN	3300 s	90 W	14.2 kN s	2.8 kg	[20]
Cold gas	100 mN	40 s	0	722 N s	3.49 kg	[21]
Chemical	400 mN	169 s	0	3.32 kN s	5.0 kg	[22]

Table 2 Assumed electrospray parameters used for comparison and resulting system performance.

System	Thrust	Specific impulse	Efficiency	Lifetime	Power	Stage impulse	Stage wet mass
Target	1.28 mN	2500 s	60%	1000 h	27 W	4.6 kN s	720 g
Reach	1.28 mN	3000 s	70%	2000 h	27 W	9.2 kN s	1000 g

V. Results

A. Structural finite element analysis

Results are presented for a wire diameter of $d = 0.25\,\text{mm}$ tensioned to 25 N which was selected as the final configuration. This wire is specified to a minimum tensile strength of 105 N. In the unloaded case the maximum deflection was the third stage circuit board bowing upwards by 0.17 mm due to the wire tension. For the 320 N lateral load design case the resulting wire tension, shown in Table 3, was 50 N giving a factor of safety of 2.1. The maximum deflection was 0.27 mm as shown in Fig. 5, resulting from the second stage being slightly lifted from the mating surface. The factor of safety for the stage structure was above four.

Table 3 Wire tension and safety factor for 320 N lateral design load.

Hold-down	$+Y$ wire	$+X$ wire	$-Y$ wire	$-X$ wire	safety factor
Stage 2	50 N	37 N	23 N	36 N	2.1
Stage 3	34 N	30 N	26 N	29 N	3.1

B. Staging separation demonstration

Staging was successfully demonstrated as seen in Fig. 6. The four hold-down wires were fused in pairs with a voltage at the lower stage input of 3.2 V and a total current of approximately 14 A, seen in Fig. 7a & b. Fusing the first pair of wires required 480 ms and a difference in fusing time of 13 ms was observed. The second pair of wires fused simultaneously after 196 ms, immediately followed by the stages separating. The difference in fuse timing was expected since the first pair of wires were not under tension and thus had to reach a higher temperature to separate.

The top-left and top-right corners of the stage reached a maximum distance of 47 mm and 53 mm respectively from their initial positions, shown in Fig. 7c. The centre of mass distance reached 49.6 mm and the stage tilted a total of

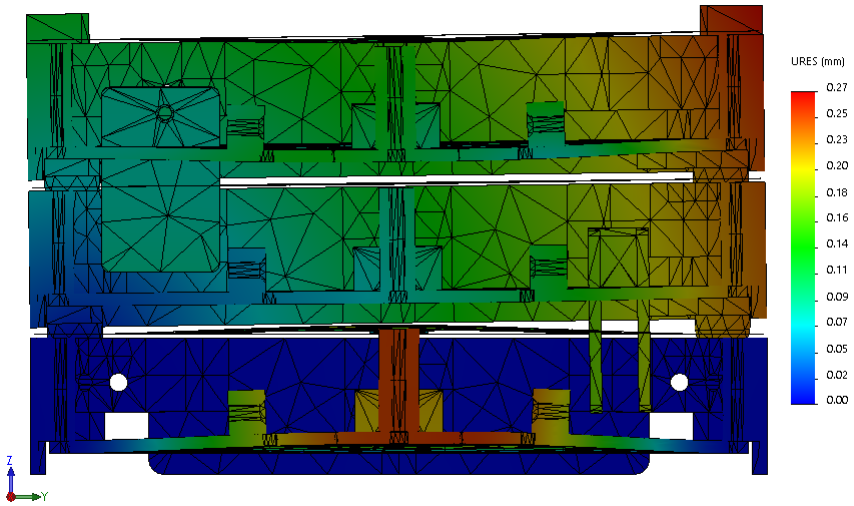

Fig. 5 Displacement for 320 N lateral design load. Exaggerated for clarity.

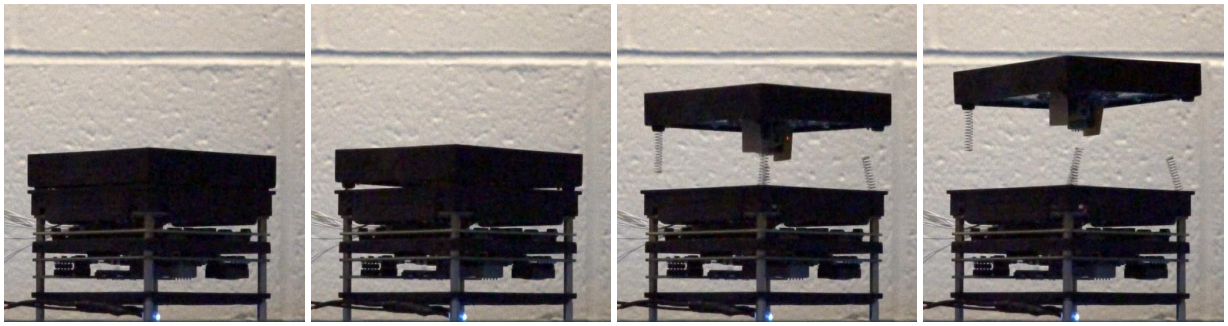

Fig. 6 Time series of staging demonstration.

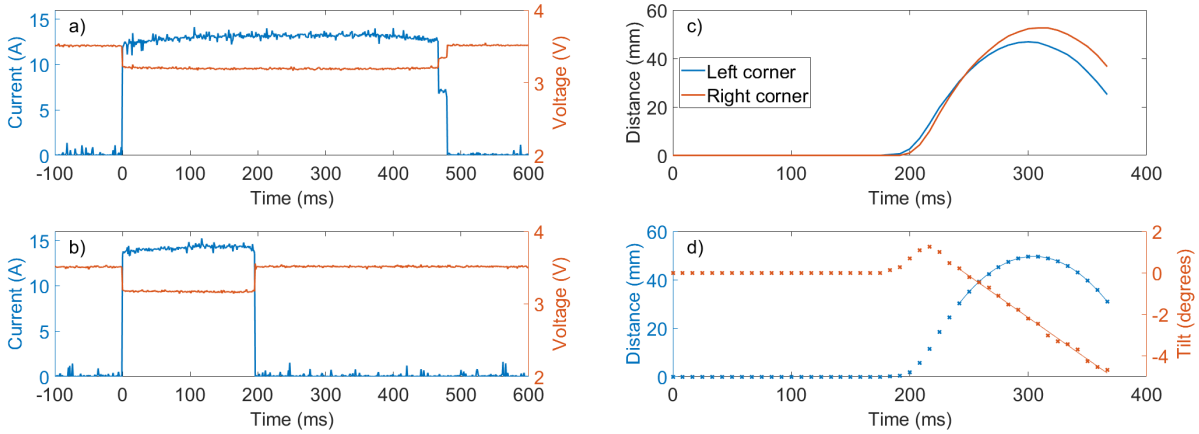

Fig. 7 Staging demonstration data. a) & b) Measured voltage and fuse current for the first and second pairs of hold-down wires respectively. c) Measured vertical motion of the stage corners. d) Centre of mass motion and tilting shown with crosses, second and first degree polynomial fits shown as thin lines during free-fall.

about 4° at a rate of 40 °/s. As seen in Fig. 6 the four separation springs behaved differently, sticking to a different stage or being ejected. This may contribute to the tip-off rate and will be resolved in the flight model by adhering the springs to the upper stage and enlarging their pockets. Table 4 relates these results to the flight model stage mass and predicts a separation speed of 0.64 m/s and a tip-off rate of 26 °/s. A typical spacecraft bus has a 20 times larger mass than the released stage, so the imparted momentum is not significant.

Table 4 Measured and scaled staging characteristics.

Staging system	Stage mass	Max distance	Sep. energy	Sep. speed	Tip-off rate
Prototype measured	84.3 g	49.6 mm	41 mJ	0.99 m/s	40 °/s
Scaled for flight	200 g	—	41 mJ	0.64 m/s	26 °/s

C. Performance scaling

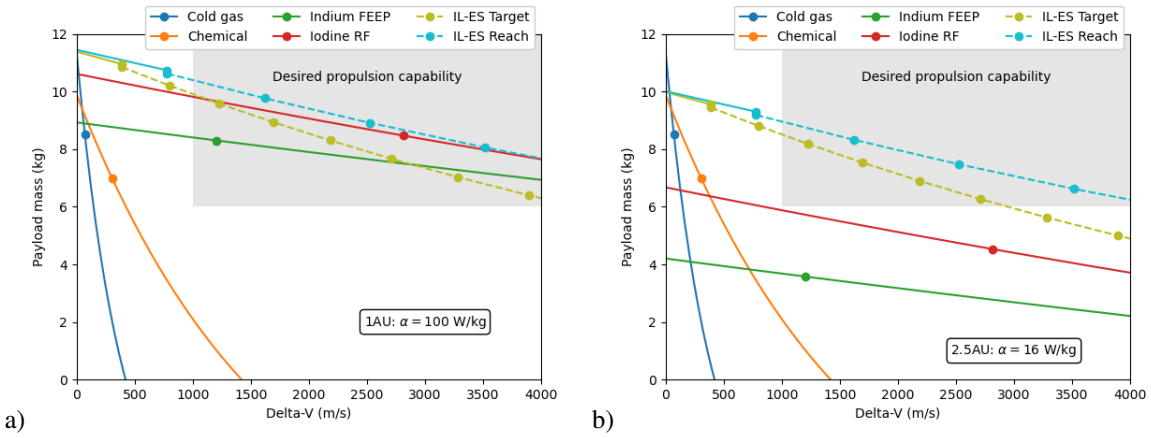

Fig. 8 Scaled performance for staged ionic-liquid electrospray (IL-ES) and state of the art systems. The dashed line is the staging extension with one dot per additional stage. a) at Earth (1 AU)**. b) In the asteroid belt** (2.5 AU)**.**

The performance of a STEP-1 based propulsion system for a 6U CubeSat is presented in Fig. 8 with a comparison to state-of-the-art systems. It is clear that electric propulsion is mandatory for high-Δv CubeSat missions. At Earth, the staged electrospray is competitive with other technologies and more nuanced differences determine the best selection. For deep-space destinations away from the Sun, such as the asteroid belt, the staged electrospray provides several kg additional payload compared to available technologies and enables previously unattainable CubeSat missions. The modest thruster performance improvement from "target" to "reach" significantly improves capability as the benefits are compounded by reducing the number of stages required.

VI. Acknowledgements

The authors thank the NASA Small Spacecraft Technology Program for their support. The work of G. Pettersson was partially supported by The Foundation Blanceflor Boncompagni Ludovisi, née Bildt. STEP-1 uses Valispace which is a browser-based collaborative engineering tool serving as a single source of truth for the project life-cycle, including requirements, design, verification, and testing.

References

[1] National Academies of Sciences, Engineering, and Medicine, *Achieving Science with CubeSats: Thinking Inside the Box*, The National Academies Press, Washington, DC, 2016. https://doi.org/10.17226/23503.

[2] Fedkiw, T., Wood, Z., Demmons, N., and Courtney, D., "Environmental and Lifetime Testing of the BET-300-P Electrospray Thruster," *Proceedings of the AIAA Propulsion and Energy Forum*, Virtual Event, 2020. https://doi.org/10.2514/6.2020-3614.

[3] Petro, E. M., Bruno, A. R., Lozano, P. C., Perna, L. E., and Freeman, D. S., "Characterization of the TILE Electrospray Emitters," *Proceedings of the AIAA Propulsion and Energy Forum*, Virtual Event, 2020. https://doi.org/10.2514/6.2020-3612.

[4] Krecji, D., et al., "Full Performance Mapping of the IFM Nano Thruster, Including Direct Thrust Measurements," *Journal of Small Satellites*, Vol. 8, No. 2, 2019, pp. 881–893.

[5] Tsay, M., Model, J., Barcroft, C., Frongillo, J., Zwahlen, J., and Feng, C., "Integrated Testing of Iodine BIT-3 RF Ion Propulsion System for 6U CubeSat Applications," *Proceedings of the 35th International Electric Propulsion Conference*, Atlanta, Georgia, 2017.

[6] Krecji, D., Reissner, A., Schönherr, T., Seifert, B., and Salem, Z., "Recent Flight Data of the IFM Nano Thruster Used for LEO Orbit Raising," *Proceedings of the 36th International Electric Propulsion Conference*, Vienna, Austria, 2019.

[7] Schoolcraft, J., Klesh, A., and Werne, T., "MarCO: interplanetary mission development on a CubeSat scale," *Space Operations: Contributions from the Global Community*, Springer, 2017, pp. 221–231.

[8] Malphrus, B. K., Freeman, A., Staehle, R., Klesh, A. T., and Walker, R., "Interplanetary CubeSat missions," *Cubesat Handbook*, edited by C. Cappelletti, S. Battistini, and B. K. Malphrus, Academic Press, 2021, pp. 85–121.

[9] Perel, J., Mahoney, J. F., Moore, R. D., and Yahiku, A. Y., "Research and development of a charged-particle bipolar thruster," *AIAA Journal*, Vol. 7, No. 3, 1969, pp. 507–511.

[10] Thuppul, A., Wright, P. L., Collins, A. L., Ziemer, J. K., and Wirz, R. E., "Lifetime Considerations for Electrospray Thrusters," *Aerospace*, Vol. 7, No. 8, 2020. https://doi.org/10.3390/aerospace7080108.

[11] Krejci, D., Jenkins, M. G., and Lozano, P., "Staging of Electric Propulsion Systems: Enabling an Interplanetary CubeSat," *Acta Astronautica*, Vol. 160, 2019, pp. 175–182. https://doi.org/10.1016/j.actaastro.2019.04.031.

[12] Jia-Richards, O., Sternberg, D. C., Grebow, D., Mohan, S., and Lozano, P. C., "Feasibility of a Deep-Space CubeSat Mission with a Stage-Based Electrospray Propulsion System," *Proceedings of the 41st IEEE Aerospace Conference*, Big Sky, Montana, 2020. https://doi.org/10.1109/AERO47225.2020.9172544.

[13] Jia-Richards, O., and Lozano, P. C., "Analytical Framework for Staging of Space Propulsion Systems," *Journal of Propulsion and Power*, Vol. 36, No. 4, 2020, pp. 527–534. https://doi.org/10.2514/1.B37722.

[14] Jia-Richards, O., and Lozano, P. C., "Laboratory Demonstration of a Staging System for Electrospray Thrusters," *Proceedings of the 36th International Electric Propulsion Conference*, Vienna, Austria, 2019.

[15] Krejci, D., and Lozano, P. C., "Micro-Machined Ionic Liquid Electrospray Thrusters for CubeSat Applications," *Proceedings of the 35th International Electric Propulsion Conference*, Atlanta, Georgia, 2017.

[16] Kristinsson, B. O., Freeman, D., Petro, E., Lozano, P. C., Hsu, A., and Young, J. A., "Operation and Performance of a Fully-Integrated Ionic-Electrospray Propulsion System," *Proceedings of the 36th International Electric Propulsion Conference*, Vienna, Austria, 2019.

[17] Jia-Richards, O., and Lozano, P. C., "Stage-Based Electrospray Propulsion System for Deep-Space Exploration with CubeSats," *Proceedings of the 40th IEEE Aerospace Conference*, Big Sky, Montana, 2019. https://doi.org/10.1109/AERO.2019.8742094.

[18] Huettl, B., and Willey, C., "Design and development of miniature mechanisms for small spacecraft," *Proceedings of the Small Satellite Conference*, 2000.

[19] *BIT-3*, Busek, 2021. URL https://www.busek.com/s/BIT3_v10.pdf, retrieved 2021-11-27.

[20] *Nano R3*, Enpulsion, 2019. URL https://www.enpulsion.com/wp-content/uploads/ENP2019-086.E-ENPULSION-NANO-R3-Product-Overview.pdf, retrieved 2021-11-27.

[21] *Micro CubeSat Propulsion System*, Vacco, 2019. URL https://cubesat-propulsion.com/wp-content/uploads/2015/11/X14102000-01_2019update.pdf, retrieved 2021-11-27.

[22] *Green Propulsion System*, Vacco, 2019. URL https://cubesat-propulsion.com/wp-content/uploads/2019/08/X19041000-Green-Propulsion-System-data-sheet-073019.pdf, retrieved 2021-11-27.